17

Multiphoton Luminescence from Gold Nanoparticles as a Potential Diagnostic Tool for Early Cancer Detection

Nicholas J. Durr, Marica B. Ericson, and Adela Ben-Yakar

CONTENTS

17.1 Introduction

Cancer is the second leading cause of death, after heart diseases [25]. It is well known that early detection of precancerous lesions can dramatically decrease morbidity and mortality [37]; thus, there is an urgent need for new diagnostic tools in order to aid in early cancer detection. More than 85% of all cancers begin as precancerous lesions that are confined to the superficial region of the epithelium [38]. However, of the currently used clinical imaging modalities, none have sufficient resolution and sensitivity to detect tumors less than a few cubic centimeters in volume [23]. The current gold standard for assessing suspicious cancerous lesions is histopathology of excised tissue biopsies. Generally the tissue biopsy is sectioned and stained before histopathological assessment. This is an invasive, labor intensive, and costly procedure. Furthermore, the accuracy of the pathological diagnosis depends on the subjective assessment of pathologists [58], which makes current tumor diagnostics ambiguous. Therefore, there is an urgent need for alternative techniques for early detection of cancer that can provide noninvasive, three-dimensional (3D), depth-resolved imaging with microscopic resolution, high sensitivity and specificity.

There are several techniques at the research stage that can meet the requirements for obtaining noninvasive imaging; however, their resolution and applicability are varying. For example, high-frequency ultrasound can image down to several millimeters deep in epithelial and connective tissue, but only provides a maximum resolution of approximately 100 μm [60]. Photoacoustic imaging is based on the photoacoustic effect in which laser pulses causing localized heating, leading to transient thermoelastic expansion and thus wideband (e.g., MHz) ultrasonic emission. The generated ultrasonic waves are then

K11937_C017.indd 309 12/21/2011 9:47:27 AM

detected by ultrasonic transducers to form images. Compared to traditional ultrasound imaging, photoacoustic imaging can provide slightly better resolution of about 50–100 μm [78,79].

Optical techniques can provide substantially better resolution. For example, optical coherence tomography (OCT) can reach resolutions of 10 μm in the lateral direction and submicron in the axial directions [16]. Other advantages of OCT include fast imaging and the capability of imaging deep into epithelial tissue—down to approximately 1 mm. OCT has found growing success in intravascular imaging over the last decade and is now being applied toward epithelial tissue imaging [24]. Confocal optical imaging technologies reject out-of-focus light to generate 3D images with diffraction-limited resolution, namely, with axial and lateral resolutions below 1 and 0.5 μm, respectively. Unfortunately, because the confocal pinhole nominally rejects all the scattered emission light, the confocal autofluorescence microscopy, using blue visible excitation light source, can generally probe intrinsic fluorophores in a very thin superficial layer of tissue that is less than 100 μm thick. Therefore, confocal autofluorescence microscopy is limited for in vivo use as a deep tissue diagnostic tool. As an alternative, confocal reflectance microscopy (CRM) based on imaging of the back-scattering of near-infrared (NIR) light is preferentially applied for improving imaging depths to several hundreds of microns in tissue [59]. However, CRM can only provide structural information with limited diagnostic capabilities. To further improve imaging depth in high-resolution optical imaging while still obtaining both molecular and structural information, nonlinear optical imaging technologies can be applied [81].

Nonlinear microscopy based on multiphoton excitation of endogenous fluorophores, so-called autofluorescence, has emerged as a novel noninvasive diagnostic tool [29,39,47]. Two-photon microscopy (TPM) was first demonstrated by Webb and colleagues in 1990 [53] and has since become the method of choice for 3D imaging of biological tissue. The quadratic dependence of the two-photon excitation process confines the fluorescence emission to the focal volume, which means that a confocal pinhole is not necessary. Unlike in confocal fluorescence microscopy, all the generated fluorescence in TPM can be collected and assumed to originate from the focal volume. More importantly, TPM utilizes NIR light through two-photon absorption process to excite UV-visible absorbing fluorophores [13,47]. In general, the mean free path length is the largest in the NIR wavelength range between 700 and 1400 nm, where the scattering is reduced and the absorption of common biological molecules is minimized [36]. The reduced attenuation in the NIR wavelengths effectively makes the tissue more transparent. Consequently, this wavelength regime generally referred to as "the optical window" of biological tissue and is preferentially used when performing optical microscopy to probe deeper layers of biological tissue. Most recently, Ben-Yakar and colleagues have shown that it is possible to image two-photon induced autofluorescence in human oral tissue biopsies down to 370 μm, reaching the theoretical imaging depths of 3–5 mean free scattering lengths [18]. Even though tissue autofluorescence enables visualizing tissue morphology, cancer diagnostics based on TPM is complex mainly due to weak signal from epidermal layers [29,56]; thus, there is a need for strategies to improve tumor contrast. In addition, the weak signal of autofluorescence makes clinical use of TPM using miniaturized endoscopes very challenging.

An alternative strategy to relying on endogenous contrast is to introduce contrast agents into the sample. The ideal optical contrast agent should provide high contrast by being very bright and targeted to the specific tumor cells, in addition to having low toxicity. Fluorescent organic dyes suffer from problems with photobleaching. Quantum dots, while exhibiting bright fluorescence and photostability, are not suitable for clinical use due to toxicity. Instead, gold nanoparticles are attractive candidates as optical contrast agents because of their bright luminescence, as well as their biocompatibility [56]. Additionally, their optical properties can be tuned in the visible and NIR wavelengths [34], allowing us to take advantage of the optical window of biological tissues.

Since the first demonstration of gold nanoparticles as sensitive probes for Raman spectroscopy [35,51], single-molecule studies [22,64,76], and as contrast agents in the electron microscopy [28], the biomedical optics community has been investigating them as sources of optical contrast for biomedical imaging. The ability to control their optical properties by engineering the particle dimensions and geometry (e.g., nanospheres or nanorods) makes them an ideal source of contrast for a variety of optical imaging modalities. Their tunability is based on the localized surface plasmon resonance effect [21]. Surface plasmon resonance arises as a result of electrons collectively oscillating along the particle surface when

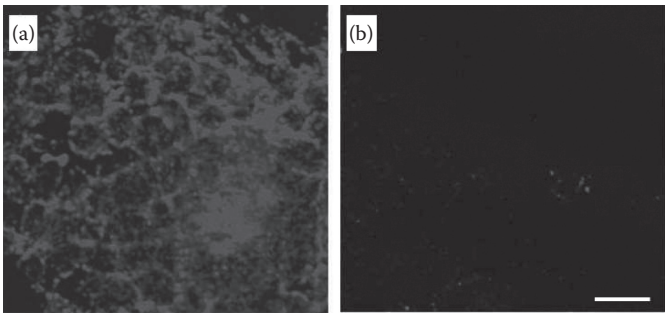

FIGURE 17.1 Laser scanning confocal reflectance images of precancerous (a) and normal fresh cervical ex vivo tissue (b) labeled with anti-EGFR gold conjugates obtained using 647 nm excitation wavelength. The same acquisition conditions have been applied to both images. The scale bar is 20 μm. (Adapted from Sokolov, K. et al., *Cancer Res*., 63, 1999, 2003. With permission.)

interacting with the incoming electromagnetic radiation. This intense interaction leads the nanoparticles to have strong absorption, scattering, and/or luminescence properties that can be utilized in providing the desired contrast mechanism for various optical imaging modalities.

One of the first uses of gold nanoparticles in combination with optical imaging of tissues was demonstrated by Sokolov et al. [66]. They applied molecularly targeted gold bioconjugates with high scattering cross sections for providing tumor contrast in CRM of human biopsies (Figure 17.1). After incubating tissue slices (200 μm thick) of fresh cervical biopsies with gold nanospheres labeled with anti-EGFR (epidermal growth factor receptor) antibodies, they successfully demonstrated molecularly targeted contrast of tumor cells overexpressing EGFR. Figure 17.1a shows the elevated reflectance signal obtained in the precancerous tissue due to the presence of gold nanospheres, as compared to normal tissue shown in Figure 17.1b. In another study, El-Sayed et al. demonstrated the use of the scattering properties of gold nanoparticles for providing cellular contrast in optical dark field microscopy [20]. Furthermore, gold nanospheres, nanoshells, and nanorods have also been applied as contrast agents for OCT [8,55,65], which also relies on scattering from the nanoparticles for a signal source.

Another approach is to use the absorption properties of gold nanoparticles to provide contrast suitable in, for example, photoacoustic or optoacoustic imaging [2,12,46,75]. The photoacoustic technique is based on detecting the acoustic signal of the expanding media caused by local heating due to laser irradiation. Therefore, the strong absorption of the gold nanoparticles drastically enhances the localized heating, and, thus, the generated photoacoustic signal is increased. Figure 17.2 presents an example from the Emelianov and colleagues [46] where targeted gold nanoparticles significantly enhance the photoacoustic signal from an in vitro model for turbid tissue (a tissue phantom). The photoacoustic

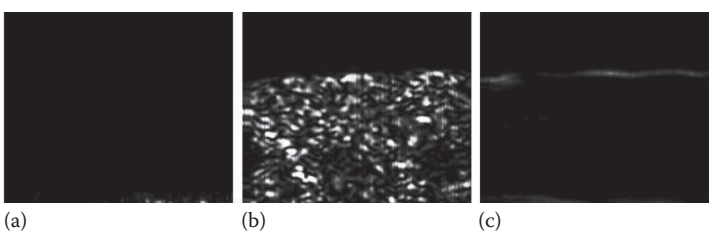

FIGURE 17.2 Photoacoustic images ($\lambda = 680$ nm) of tissue phantoms consisting of A431 epithelial skin carcinoma cells: (a) unlabeled control, (b) targeted phantom exposed to anti-EGFR conjugated gold nanoparticles (50 nm), and (c) phantom exposed to nontargeted gold nanoparticles (50 nm). The images measure 2×1.67 mm. The faint signal in the lower region of the images in (a) and (c) seems to be due to absorption of the laser by the plastic bottom of the Petri dish holding the phantom. (Adapted from Mallidi, S. et al., *Opt. Express*, 15, 6583, 2007. With permission.) AQ2

signal is nearly undetectable when no particles are present (Figure 17.2a), while the signal from cancer cells are clearly visible when labeled with gold nanoparticles functionalized with anti-EGFR (Figure 17.2b). Interestingly, they also demonstrate the possibility of using wavelength tuning, to preferentially generate signal from particles which are bound to cells. As shown by Figure 17.2c, the signal obtained from the tissue phantom exposed to nontargeted gold nanoparticles, i.e., particles without anti-EGFR, is very low, which is explained by a redshift in the absorption spectrum of the functionalized particles. In addition to photoacoustic imaging, the strong light absorption of gold nanoparticles can be used for photothermal therapy [19], which is an intriguing research field in itself and will not be covered in this chapter.

When it comes to providing contrast for nonlinear optical imaging, it is instead the bright photoluminescence from the gold nanoparticles becomes an attractive optical property to be utilized [6,9,15,17,33,49,73,77]. Gold nanorods are particularly appealing because their longitudinal plasmon modes are resonant in the NIR range, where the absorption of water and biological molecules is minimized [67]. The potential of gold nanorods for in vivo nonlinear optical imaging was first demonstrated by Cheng and colleagues [44,72]. They presented real-time noninvasive imaging of blood flow in a mouse ear using the multiphoton luminescence (MPL) from the nanorods. In another in vivo study, Tunnell and colleagues demonstrate the possibility of using MPL for enhancing the signal when performing tumor imaging using nonlinear microscopy. In this study, they administered gold nanoshells to murine tumors and compared the MPL images to autofluorescence signal [57]. These studies demonstrate the capability of gold nanoparticles as contrast agents in nonlinear optical microscopy; however, in order to provide tumor selectivity, the particles need to be targeted. Thus, our strategy is to adopt the tumor targeting protocol already implemented for other imaging modalities discussed earlier and combine with the strong MPL signal of gold nanorods, to provide tumor contrast. We here demonstrate the technology on experimental tissue phantoms and show that one to two orders of magnitude less excitation power are required when imaging labeled tumor cells compared to utilizing the autofluorescence, proving the strong brightness of gold nanorods when illuminated with femtosecond laser pulses at their resonance. In addition, we investigate the toxicity of the gold nanorods.

17.2 Materials and Methods

17.2.1 Preparation of Gold Nanospheres

We prepared gold nanospheres using the method introduced by Turkevich and colleagues in 1953 [71]. The method is based on reducing a solution consisting of gold chloride using sodium citrate which causes the auric ions to nucleate and form particles. The size distribution of the formed nanoparticles is dependent on the kinetics of the process. The diameter of the nanospheres was measured to be 50 nm with a linear absorption peak of 530 nm.

17.2.2 Preparation of CTAB-Coated Gold Nanorods

The synthesis of gold nanorods generally starts from small gold seeds (1.5–3 nm) [48,62], but their anisotropic growth is promoted by adding cationic surfactant (hexadecyltrimethylammonium bromide, CTAB), silver ion, and ascorbic acid to the solution. The CTAB and silver atoms prefer to be adsorbed on the sides of the rods rather than at the edges, which leads to the deposition of gold atoms only on the edges and, subsequently, the formation of the desired gold nanorods. The CTAB molecules also play an important role as a stabilizer for dispersion in an aqueous phase by forming a bilayer on the gold nanorod.

In this study, we synthesized CTAB-coated gold nanorods using this seed-mediated, surfactant-assisted growth method introduced earlier. Colloidal gold seeds (1.5 nm diameter) were first prepared by mixing aqueous solutions of CTAB (0.1 M, 9.75 mL) and hydrogen tetrachloroaurate(III) hydrate (0.01 M,

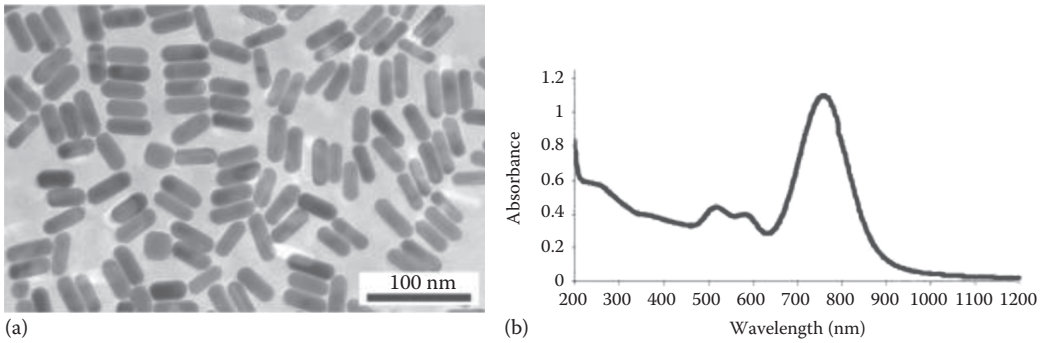

FIGURE 17.3 Properties of CTAB-coated gold nanorods used as contrast agents. (a) TEM image of the produced gold nanorods indicates an average length and width of 48 ± 6 and 14 ± 2, respectively. (b) The corresponding absorbance spectrum of the gold nanorods in aqueous solution. The absorption peaks at 754 and 520 nm correspond to the longitudinal and latitudinal resonance, respectively.

250 μL). For nanorods to form, we found it necessary to use low-purity CTAB from Fluka (96% purity)* [17]. An aqueous solution of sodium borohydride (0.01 M, 600 μL) was added, and the colloidal gold seeds were injected into an aqueous "growth solution" of CTAB (0.1 M, 9.5 mL), silver nitrate (0.01 M, varying amounts of silver between 20 and 120 μL depending on desired nanorod aspect ratio), hydrogen tetrachloroaurate(III) hydrate (0.01 M, 500 μL), and ascorbic acid (0.1 M, 55 μL). Nanorods were purified by several cycles of centrifugation and resuspension in ultrapure water. They were then isolated in the precipitate, and excess CTAB was removed in the supernatant.

We characterized the physical dimensions of the formed gold nanorods with transmission electron microscopy (TEM) and measured the average aspect ratio of the nanorods as 3.4 ± 0.6. We air dried a 2 μL volume from the stock solution of each sample on a copper grid from Grid Tech© (Cu-400CN). Imaging was performed on Hitachi S-5500 TEM at 150 k magnification. A representative image is shown in Figure 17.3a. Figure 17.3b shows that the longitudinal plasmon mode of these nanorods was centered at 754 nm and the lateral resonance around 520 nm wavelengths.

17.2.3 Preparation of PEGylated Gold Nanorods

Given the known cytotoxicity of CTAB surfactant coating, we also explored labeling with a more biocompatible coating, PEG-coated gold nanorods. In this case, we purchased gold nanorods having the dimensions 39 ± 6 nm × 9 ± 1 nm that were coated with neutravidin-terminated PEG [Ntherapy Gold Nanorods, Nanopartz]. The exact size the PEG used in the CTAB dialysis is a trade secret, but the manufacturer did specify that it is less than 5 kDa.

17.2.4 Molecular Targeting of Nanorods Using Antibodies

To obtain molecularly specific targeting of the CTAB-coated gold nanorods, we functionalized the nanorods by adsorbing anti-EGFR antibodies (clone 29.1, Sigma) to the surface of the nanorods. In this protocol, the positive surface potential of the gold nanorods was converted to a negative potential by coating the CTAB nanorods with polystyrene sulfonate (PSS). PSS (MW 14 kD, 10 mg/mL in AQ4

* The CTAB source was found to be critical for success in the gold nanorod synthesis. For nanorods to form using the published procedures, it was necessary to use lower-purity CTAB. CTAB from both Fluka (96% purity) and MP Biomedical (98% purity) resulted in formation of gold nanorods; however, production of nanorods was not possible using CTAB obtained from the following manufacturers: Acros (99% purity), Aldrich (100% purity), and Sigma (99% purity). We speculate that this difference is due to degree of purity of the CTAB, but cannot fully understand the reason. However, reviewing the literature, it is clear that gold nanorod syntheses have only been reported using the CTAB of lower purity from either Fluka or MP Biomedical.

1 mM NaCl solution) was added to the nanorod suspension in a 1:10 volume ratio and allowed to react for 30 min. The particles were collected via centrifugation at 2000 g for 30 min, resuspended in NaCl (1 mM), and reacted with another aliquot of PSS solution. Following the second PSS incubation, the particles were washed twice in water and then resuspended in HEPES (40 mM, pH 7.4) for compatibility with the antibody solution. Anti-EGFR antibody was purified using 100 kD MWCO filters (Centricon) and resuspended in HEPES (40 mM, pH 7.4, 200 μg/mL). Antibody solution and nanorods were mixed at 1:1 volume ratio and allowed to interact for 45 min. Polyethylene glycol (PEG, MW 15 kD, 10 mg/mL in 1× PBS) was then added for stability, and the nanorods centrifuged to remove unbound antibodies. For the control, nanorods with unspecific PEG coating were used.

To conjugate the PEG-neutravidin-functionalized gold nanorods, we used biotin-labeled antibodies for EGFR (clone 111.6, MS-378-B0, Thermo Scientific). The density of the stock antibody solution was 200 μg/mL, and the size of an individual antibody is 145 kDa, which gives an approximate antibody density of 8.3×10^{14} antibodies/mL. We mixed the GNR808p, antibody, and 40 mM HEPES solution at a 1:1:4 volume ratio, which results in an interaction of ~67 antibodies for every nanorod. The mixture was allowed to interact for 20 min and then centrifuged at 2000 × g for 30 min to remove unbound antibodies. We performed a second washing step, resuspending the pellet in 2 mL of 40 mM HEPES, and centrifuging at 2000 × G for 30 min to further remove unbound antibodies.

17.2.5 Tissue Models

In this work, the targeted gold nanorods were demonstrated as potential contrast agents using two model systems: (1) monolayer of cancer cells (either EGFR-overexpressing A431 human epithelial skin cancer cells, American Type Culture Collection, or MDA-MB-468 human epithelial breast cancer cells) and (2) 3D tissue phantoms. The 3D tissue phantoms were prepared from A431 skin cancer cells cultured in DMEM supplemented with 5% fetal bovine serum (FBS, Sigma) incubated at 37°C in a humidified 5% CO_2 incubator. Cells were harvested via trypsinization and resuspended in PBS at a concentration of 6×10^6 cells/mL. The cell suspension was mixed with either EGFR-targeted or PEG-coated nanorods in a 1:1 volume ratio and allowed to interact for 45 min. The cells were then spun down at 200 g for 5 min to remove unbound nanorods. The cells were resuspended in a buffered collagen solution at a concentration of 7.5×10^7 cells/mL. The collagen/cell mix was pipetted into a 500 μm well (Molecular Probes) and sealed with a coverslip for imaging.

17.2.6 Multiphoton Microscopy Imaging System

The MPL imaging in our studies is performed using two different home-built multiphoton microscopy systems, one inverted and the other upright. Both systems were connected to a Ti:sapphire, mode-locked laser oscillator (MaiTai, Spectra Physics, Newport). This source has a repetition rate of 80 MHz, an excitation wavelength, λ_x, tunable from 710 to 880 nm, and an average power, P_{ex}, of 0.6–1.1 W across the tuning range. The full width at half maximum (FWHM) of the spectral bandwidth, $\Delta\lambda$, was measured to be 7.5 nm. Using a time-bandwidth product of 0.44, a transform-limited pulse with this bandwidth would have an FWHM pulse duration, FWHM τ_p^{FWHM}, of 120 fs. We measured the $1/e^2$ diameter of the excitation beam to be approximately 1.5 mm in the vertical direction and 1.2 mm in the horizontal direction at the output of the laser oscillator. The slightly larger divergence of the smaller (horizontal) axis resulted in the beam shape being relatively circular at the position of the objective back aperture. We used two lenses in a Galileo-configuration beam expander with focal lengths of 30 and 75 mm for a 2.5× increase in beam size. Two sets of half-wave plate and polarizing beam cube are used to control the excitation power. In all experiments, the laser was operated at 760 nm.

We used the inverted microscope for single-cell-layer experiments, presented in this chapter. Figure 17.4 shows a schematic drawing and a photo of the inverted setup. The laser light is raster scanned into the back aperture of a high-NA oil immersion objective lenses (Zeiss 63×/1.4 and Olympus 40×/1.3) with a set of galvanometric scanning mirrors (6215H, Cambridge Technologies). Emitted

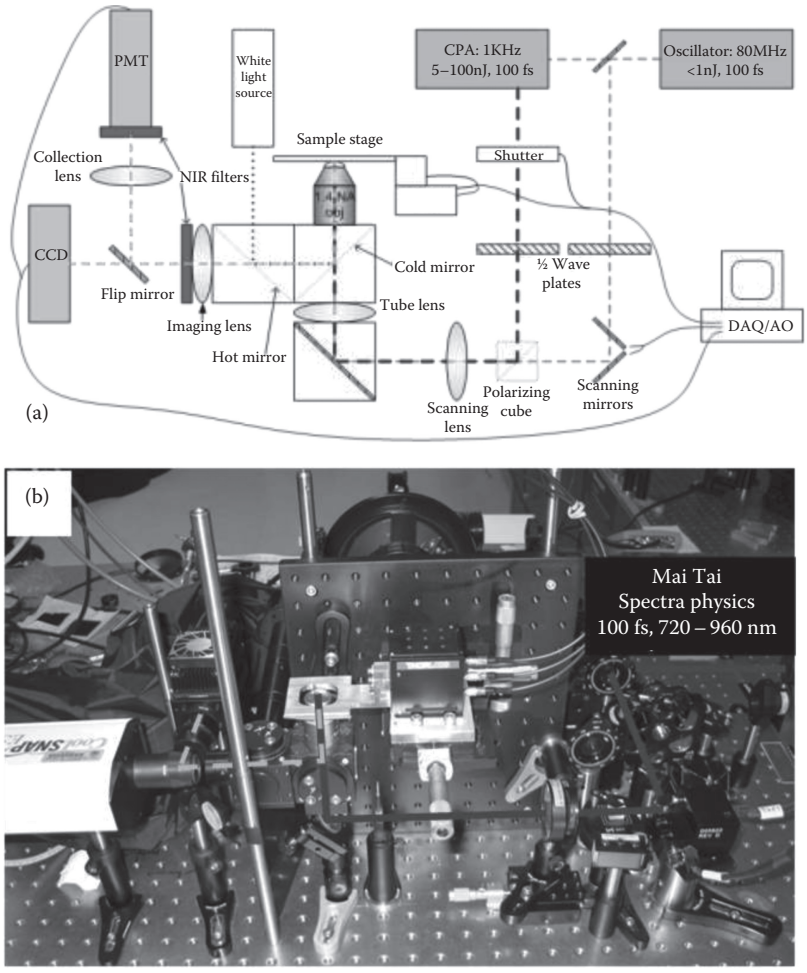

FIGURE 17.4 The inverted laser scanning microscope for nonlinear imaging. (a) Schematic with labeled parts. (b) Photograph of actual microscope. The lateral and axial resolutions are 320 and 625 nm, respectively, using the oil immersion, 1.4 NA, 63× Zeiss objective.

light is epi-collected, reflected by a cold mirror (400–700 nm reflectance, HT-1.00, CVI Laser), passed through a laser filter (BG-38, Schott, blocks > 700 nm), detected with a cooled GaAsP photomultiplier tube (PMT) (H7422-40, Hamamatsu), and assembled into an image in real time with a data acquisition card (6111E, National Instruments). Given the response of the PMT and optics used, the system collects emission light between 400 and 700 nm. The scan area at each image plane is variable to sizes up to 150 × 150 μm. The field of view can be scanned into a 512 × 512 pixel image at a rate of 1.5 frames per second. The sample can be moved in the axial direction with a piezoelectric actuator (P280, Physik Instrumente).

We used the upright microscope for phantom experiments, presented in this chapter. Figure 17.5 shows a photo and schematic drawing of the upright multiphoton microscope. The excitation path consists of a pair of scanning mirrors, two relay lenses, dichroic mirror, and a long working distance, large field-of-view objective lens (20×/0.95 water dipping objective, Olympus). The emission path uses non-descanned collection, large diameter optics, high-throughput filters, and a sensitive PMT to maximize visible-light sensitivity. A customized computer program controls and synchronizes image acquisition, mirror scanning, excitation power control, and sample position. The microscope is configured in an upright configuration—the sample is placed under the objective—to enable the use of a water dipping

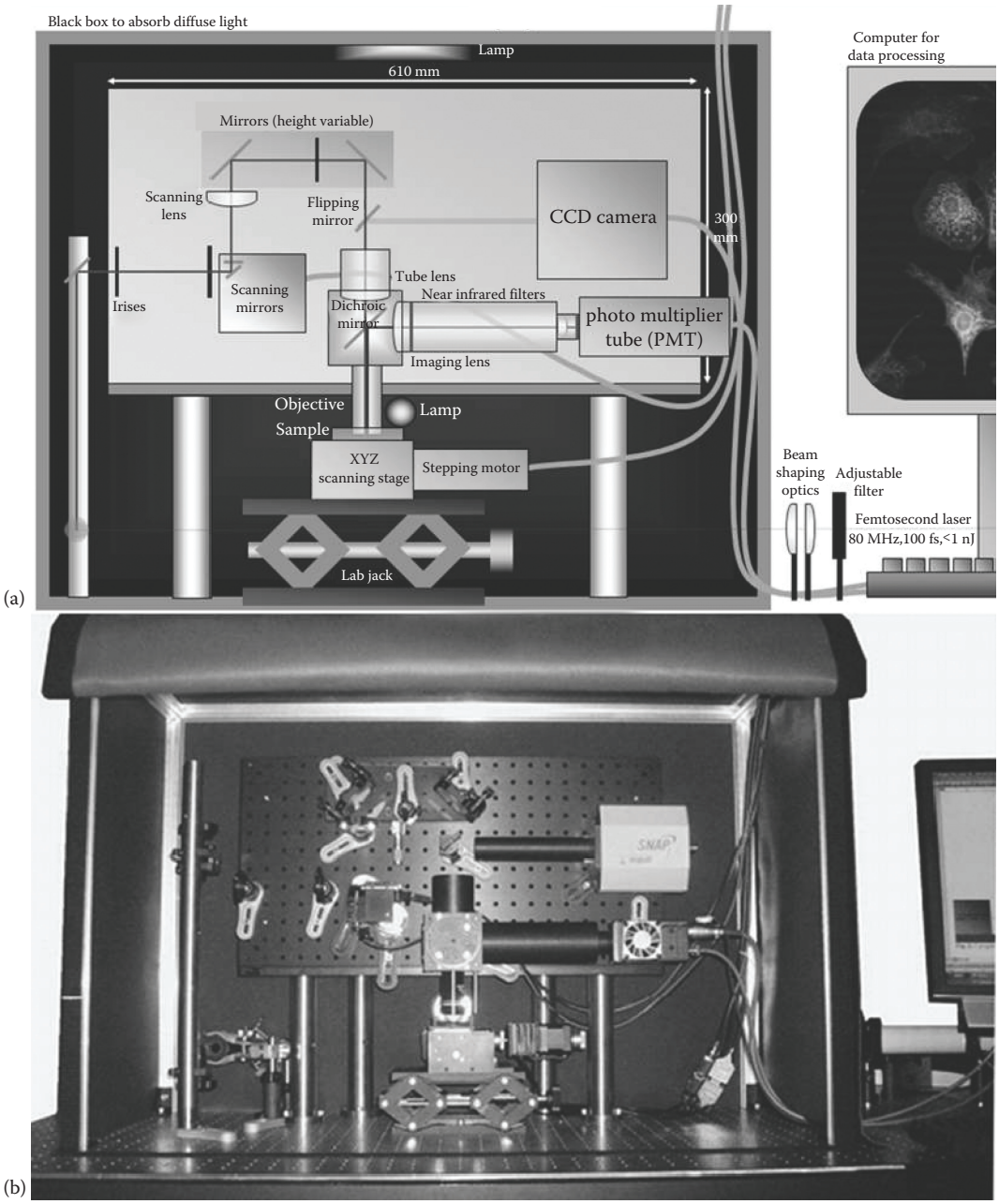

FIGURE 17.5 The upright laser scanning microscope for deep nonlinear imaging. (a) Schematic with labeled parts. (b) Photograph of actual microscope. The lateral and axial resolutions are 320 and 625 nm, respectively, using the water dipping, 0.95 NA, 40× Olympus objective.

objective and to facilitate future studies involving in vivo animal studies. Imaging is typically performed at 1×10^6 pixels per second to match the bandwidth of our preamplifier. This setup was used for deep imaging experiments with the tissue phantoms [18].

17.2.7 Toxicity Assay

We performed the toxicity test of the biocompatibility of the gold nanorods using an MTT assay (Promega CellTiter Aqueous One kit). Here, the proliferation of A468 cancer cells was assessed after incubation with either CTAB-coated or PEG-coated gold nanorods at different concentrations for 24 and 48 h. At each time point, the density of cells incubated with each solution was compared to the density of cells incubated in DMEM supplemented with 5%–10% FBS. Concentrations in the range 4–4000 pM were investigated, and around 100 pM was found sufficient for dense labeling of the cells.

17.3 Results

Here, we present the bright MPL properties of gold nanorods labeling cancer cells, as an attractive method to potentially improve tumor contrast for noninvasive diagnostics. First, we present data to demonstrate how the bright MPL significantly increases the signal obtained from nonlinear imaging of individual cancer cells labeled with molecularly targeted gold nanorods. We then present data validating that CTAB-produced gold nanorods can be made biocompatible, by capping the particles with PEG. Finally, we demonstrate the potential of MPL from molecularly targeted gold nanorods as a diagnostic tool in a tissue phantom consisting of cancer cells embedded in a collagen matrix, to simulate in vivo tissue.

To show the bright luminescence properties of gold nanorods, we present in Figure 17.6 a comparison between the properties of two-photon autofluorescence images of unlabeled cells and MPL images of nanorod-labeled human carcinoma skin cells (A431). Unlabeled cells show a relatively uniform distribution of two-photon-induced autofluorescence signal throughout cellular cytoplasm (Figure 17.6a), using a laser power of 9 mW. On the other hand, images of the cells, labeled with EGFR-targeting gold nanorods, show signal mainly in the periphery of the cells and interestingly can be acquired using much less laser excitation powers, as low as 0.14 mW (Figure 17.6b). At these low powers, the unlabeled cells cannot be visualized at all (Figure 17.6c). The bright rings observed in the cells labeled with functionalized gold nanorods are consistent with the expected distribution of

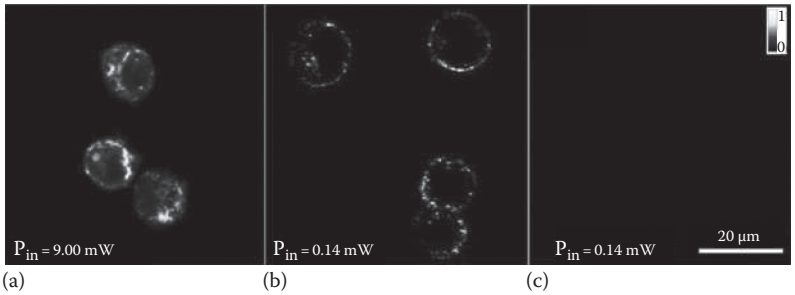

FIGURE 17.6 Multiphoton images of A431 cancer cells without and with labeling of EGFR-targeted gold nanorods (length = 48 nm, width = 14 nm) as imaged using the inverted microscope with an oil immersion 63×/1.4 objective lens and 760 nm excitation wavelength. (a) Two-photon autofluorescence image of unlabeled cells requires 9.00 mW of average laser excitation power. (b) MPL images of cells labeled with EGFR-targeted gold nanorods can be obtained using as little as 0.14 mW of average laser excitation power. The need for 64 times less power to generate the same signal level indicates that MPL from nanorods can be more than 4000 times brighter than two-photon autofluorescence from intrinsic fluorophores. (c) Two-photon autofluorescence image of unlabeled cells does not generate any signal at 0.14 mW of average laser excitation power used to obtain MPL images.

EGFR at the cellular membrane and have been reported also in confocal reflectance imaging using spherical gold nanoparticles [66]. This result therefore indicates successful labeling and confirms that the signal is coming directly from the multiphoton-induced luminescence of gold nanorods. There are also several discrete bright spots in the cytoplasm of nanorod-labeled cells that are indicative of endosomal uptake of labeled EGFRs inside cells [4,63]. Taken together, these results imply that the cells, labeled with functionalized gold nanorods, can be visualized using 64 times less power compared to autofluorescence to obtain similar signal levels, and prove the potential of the nanorods as bright contrast agents for tumor diagnostics.

To find the optimal excitation wavelength used for excitation of the gold nanorods, we tuned the laser excitation wavelength from 710 to 910 nm (data not presented) and found that 760 nm yielded the brightest MPL signal from the nanorods. This excitation wavelength corresponds to the longitudinal plasmon resonance frequency of the nanorods (Figure 17.3b) and also coincides with the optimal excitation wavelength of autofluorescence of the cells. The intrinsic fluorophores, such as NAD(P)H, flavins, retinol, and tryptophan, are mainly responsible for the autofluorescence as they have two-photon cross sections that increase with decreasing excitation wavelength from 1000 to 750 nm, and level off around 750 nm [80]. The similarity of the optimal excitation wavelengths for both the gold nanorods and cellular autofluorescence allows a comparison of the two imaging modalities under identical excitation conditions. As we showed earlier, MPL imaging of nanorod-labeled cells requires 64 times less power than the autofluorescence of unlabeled cells in order to achieve the similar collected intensity (Figure 17.6). Given the quadratic dependence of emission intensity on the incident power, this observation implies that, for equal excitation powers, MPL imaging of nanorod-labeled cancer cells can generate more than 4000 times larger emission signal than two-photon autofluorescence imaging of unlabeled cells.

CTAB is known to be cytotoxic at the concentrations used in nanorod labeling, raising concerns about the in vivo use of nanorods for molecular imaging [32,69,70]. To alleviate cytotoxicity concerns, CTAB can be exchanged with PEG, a much more biocompatible material, in a dialysis reaction [52]. In this study, we compare the biocompatibility of CTAB-coated gold nanorods and PEGylated gold nanorods in a cell viability assay (Figure 17.7). This comparison also incorporates gold nanospheres since they are synthesized without CTAB and are expected to show no significant cytotoxic effects. Indeed, the CTAB-coated nanorod samples exhibit significant cytotoxicity within 24 h at concentrations of 400 pM and above. For longer incubation times, above 48 h, even concentrations as low as 40 pM show cytotoxic effects. On the other hand, we observe that this toxicity problem can be eliminated by using PEGylated gold nanorods. As Figure 17.7 indicates, the PEGylated nanorods have very low cytotoxicity at all concentrations after 24 h of incubation. After 48 h exposure, only small effects on cell proliferation are observed and only at the highest concentration 4000 pM (data not shown). These results which are in agreement with other studies [61] emphasize the importance of taking toxicity into consideration in order to avoid unwanted toxic effects using gold nanorods as contrast agents. We can conclude that PEG coating should be preferentially used to avoid unspecific toxicity.

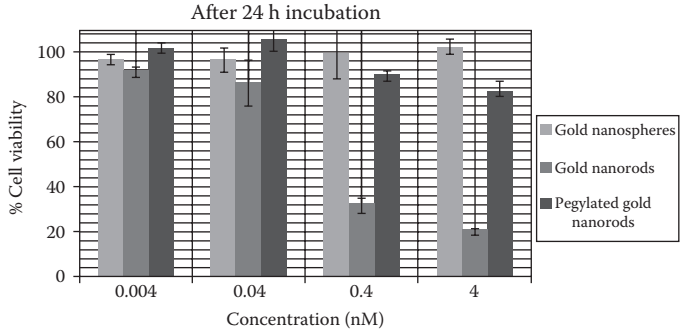

FIGURE 17.7 Cell viability of A468 cancer cells, exposed to various concentrations of gold nanospheres, CTAB-coated gold nanorods, and PEGylated gold nanorods for 24 h, is assessed using MTT assay. While the CTAB-coated nanorods exhibit strong cytotoxicity above 0.4 nM, the PEGylation is shown to drastically reduce cell death.

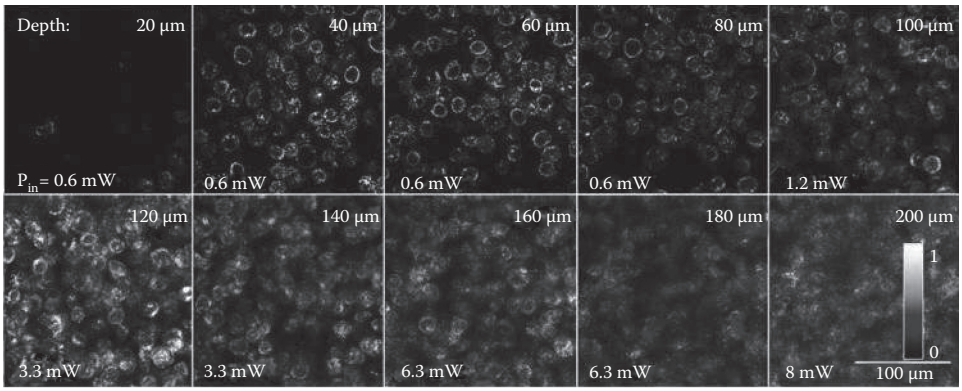

FIGURE 17.8 MPL images of a tissue phantom, consisting of cancer cells that are labeled with anti-EGFR-targeted nanorods as contrast agents and embedded in a collagen matrix. Imaging was performed using the upright microscope with a 20×/0.95 NA water dipping objective, allowing deep tissue imaging. The laser excitation power was increased to maintain constant emission intensity at each imaging depth.

To test the potential of the targeted gold nanorods not only to elevate the luminescence signal of a few cells but also luminescence of tissue, we used 3D cellular tissue phantom, mimicking epithelial tissue. The tissue phantom is constructed by human cancer cells (A431) that are labeled with targeted gold nanorods and embedded in a collagen matrix. Here, we used the upright microscope with long working distance, water dipping objective to facilitate deep tissue imaging because the inverted microscope limits its imaging depths to a few tens of microns due to the spherical aberrations and short working distance of the oil immersion objective. Figure 17.8 shows the MPL signal of the tissue phantom obtained at different depths by performing optical sectioning. The increased PMT gain configuration used in this experiment allowed imaging at 10 times less power than the single-cell-layer experiments presented in Figure 17.6. To maintain a constant detected intensity throughout the phantoms, we increased the power when imaging deeper into the phantom. Even with the addition of gold nanoparticles or nanorods, the tissue extinction coefficient is dominated by the tissue scattering. Based on our calculations (unpublished data), the mean free path of a 780 nm photon in epithelial tissue only modestly decreases from 99 to 98 μm, when comparing the two different cases without or with the presence of nanorods. This approximate calculation is consistent with our experiments in which we observed no significant change in extinction coefficient in gold-nanorod-labeled tissue phantoms [17]. The ability to perform imaging down to a depth of 200 μm demonstrates the potential of gold nanorods to be used as contrast agents without inflicting on the maximum imaging depth achievable in biological tissue when performing TPM for in vivo imaging and tumor diagnostics.

17.4 Discussion

Here, we demonstrate the potential of gold nanorods as bright nonlinear plasmonic contrast agents based on MPL for molecularly targeted imaging of cancer cells. By functionalizing gold nanorods with anti-EGFR antibodies, we can molecularly target the cancer cells. The three orders of magnitude brighter signal of gold-nanorod-labeled cells as compared to the cell autofluorescence imply that we need much less laser excitation powers for in vivo imaging. This technique, therefore, has the potential to selectively diagnose tumor cells as the nanorod-targeted tumor cells will appear much brighter compared to the low-autofluorescence, unlabeled background cells, although this experiment still needs to be demonstrated.

Within the last couple of years, nonlinear microscopy has gained elevated attention because of its potential for becoming a noninvasive diagnostic tool [14,40,56]. While two-photon-induced autofluorescence of tissue may provide some contrast due to the presence of intrinsic fluorophores, such as

NAD(P)H, flavins, retinol, and tryptophan, it exhibits weak emission due to the small values of the two-photon absorption cross sections on the order of 10^{-4} to 10^{-1} GM [80,81]. Second harmonic generation (SHG) imaging, being a nonlinear scattering process, can also provide contrast to native structures in biological tissues; however, it is restricted to fibrillar structures, such as collagen, axons, muscle filaments, and microtubule assemblies [11].

Exogenous fluorophores could potentially be used as alternative contrast agents to nonlinear imaging with only intrinsic fluorophores. Among the brightest of these fluorophores, some organic dyes have two-photon action cross sections on the order of 10–100 GM [3,74,81]. Also quantum dots are being considered as two-photon contrast agents, and extremely large two-photon cross sections of up to 50,000 GM have been reported [42]. However, problem with toxicity is the major obstacle of developing organic dyes or quantum dots to potential clinically applicable contrast agents. Instead, gold nanoparticles have been shown to have minimal cytotoxic effects and are believed to be relatively biocompatible [1,43]. We here demonstrate that PEG coating of CTAB-produced gold nanorods enhances their biocompatibility with cultured cancer cells.

Our measurements of gold nanoparticle brightness indicate that the effective two-photon absorption cross section of gold nanorods can be as high as 10^6 GM (unpublished data). Historically, the large multiphoton absorption cross-section values observed in metallic particles were somewhat unexpected. Instead, gold particles were known for their quenching of fluorescence rather than exhibiting fluorescence emission [41]. The lifetime of excited electrons in metals is extremely fast, on the order of tens to hundreds of femtoseconds [7,68], leading to very short emission lifetimes, on the order of 10^{-10} s [10]. Nonetheless, weak luminescence can be obtained. Single-photon-induced luminescence from bulk copper and gold was first reported in 1969 [50]. Later, it was found that roughened metal surfaces exhibited much higher luminescence efficiency than smooth surfaces [10]. In 2000, it was found that gold nanorods offered dramatically larger quantum yield than bulk gold, which was dubbed, the "lightning rod" effect [49]. The results presented here support the hypothesis that the presence of a surface plasmon resonance is important to the efficient generation of luminescence from gold nanorods.

As gold nanorods exhibit intense optical interaction properties when excited at their plasmon resonance, they can preferably be utilized to improve contrast for nonlinear optical technologies. Furthermore, the use of bright contrast agents instead of the dim endogenous fluorophores can enable imaging using clinically relevant nonlinear endoscopes that are less efficient [29,30]. Thus, the large brightness of gold nanoparticles can enable molecularly specific imaging in systems with poor collection efficiencies and/or limited excitation fluence, such as that typically found in nonlinear endoscopic probes [12–15].

17.5 Future Trends

To achieve molecularly specific nonlinear imaging of tissues with plasmonic contrast agents, several challenges remain. The biggest disadvantage of using gold nanoparticles as contrast agents is their large AQ5 size. While some groups have had success in the topical application of gold nanoparticles by using permeation enhancers, such as chitosan [26], the delivery of gold nanoparticles, which are orders of magnitude larger than molecular fluorophores, remains a challenge. Therefore, more detailed studies exploring the topical delivery and biodistribution of gold particles are necessary to understand the true biocompatibility of this class of contrast agents. In addition, further studies on clearance of the compounds are important.

While the large size of gold nanoparticles makes topical delivery and clearance challenging, it can actually be advantageous when it comes to intravascular delivery and plasmonic photothermal treatment [31]. Because of the leaky vasculature phenomenon, their large size may allow preferentially delivering them to the regions of tumors [54]. Their large size may also be beneficial in preferentially heating the nanorods. There has been indeed important progress in using gold nanoparticles as therapeutic agents, based on the large absorption of gold nanoparticles at NIR wavelengths for targeted thermal therapy

[19,27,31,45,53,54]. Excitation of nanoparticles with ultrashort laser pulses opens the possibility for additional novel laser therapies [5]. Thus, a highly interesting future direction is the combination of diagnostic and therapeutic agents, in the so-called theragnostic contrast agent [57].

In conclusion, we here demonstrate the potential of the combination of nonlinear optical microscopy and molecularly targeted gold nanorods for high-resolution diagnostic imaging of cancer cells. By the use of nonlinear optical microscopy techniques based on femtosecond laser pulses operating in the optical window of tissue in the NIR wavelength region, we can perform deep tissue imaging as demonstrated by the 3D tissue phantoms. While endogenous fluorophores can visualize tissue morphology, enhanced tumor contrast is desirable, which we obtain using gold nanorods that exhibit bright MPL and can be molecularly targeted by conjugation to cancer-specific moieties such as antibodies. With some further refinement, the technique perhaps has its most important application for noninvasive multiphoton endoscopic diagnostics as improved tumor contrast and bright signal will here overcome the poor collection efficiencies with these types of miniaturized instruments.

ACKNOWLEDGMENTS

The authors acknowledge support from the National Science Foundation under grants BES-0548673, CBET-1014953, and Career Award, CBET-0846868, a grant from the Texas Ignition Fund by The University of Texas Board of Regents, and VINNOVA (2008-03414, Sweden).

REFERENCES

1. Abrams, M. J. and B. A. Murrer. 1993. Metal compounds in therapy and diagnosis. *Science* **261**:725.
2. Agarwal, A., S. W. Huang, M. O'Donnell, K. C. Day, M. Day, N. Kotov, and S. Ashkenazi. 2007. Targeted gold nanorod contrast agent for prostate cancer detection by photoacoustic imaging. *Journal of Applied Physics* **102**:064701.
3. Albota, M. A., C. Xu, and W. W. Webb. 1998. Two-photon fluorescence excitation cross sections of biomolecular probes from 690 to 960 nm. *Applied Optics* **37**:7352.
4. Barnes, C. J. and K. Rakesh. 2004. *Biology of the Epidermal Growth Factor Receptor Family*, Vol. 119. Springer, New York.
5. Ben-Yakar, A., D. S. Eversole, and O. Ekici. 2008. Spherical and anisotropic gold nanoparticles in plasmonic laser phototherapy of cancer. In C. Kumar (ed.), *Non-Magnetic Metallic Nanomaterials for Life Sciences of the 10 Volume Series on Nanomaterials for Life Sciences*. John Wiley & Sons, Weinheim, Germany, pp. 493–539.
6. Beversluis, M., A. Bouhelier, and L. Novotny. 2003. Continuum generation from single gold nanostructures through near-field mediated intraband transitions. *Physical Review B* **68**:115433.
7. Biagioni, P., M. Celebrano, M. Savoini, G. Grancini, D. Brida, S. Matefi-Tempfli, M. Matefi-Tempfli, L. Duo, B. Hecht, G. Cerullo, and M. Finazzi. 2009. Dependence of the two-photon photoluminescence yield of gold nanostructures on the laser pulse duration. *Physical Review B* **80**:045411.
8. Boppart, S. A., A. L. Oldenburg, C. Xu, and D. L. Marks. 2005. Optical probes and techniques for molecular contrast enhancement in coherence imaging. *Journal of Biomedical Optics* **10**:41208.
9. Bouhelier, A., M. R. Beversluis, and L. Novotny. 2003. Characterization of nanoplasmonic structures by locally excited photoluminescence. *Applied Physics Letters* **83**:5041.
10. Boyd, G. T., Z. H. Yu, and Y. R. Shen. 1986. Photoinduced luminescence from the noble metals and its enhancement on roughened surfaces. *Physical Review B, Condensed Matter* **33**:7923. AQ6
11. Brown, E., T. McKee, E. diTomaso, A. Pluen, B. Seed, Y. Boucher, and R. K. Jain. 2003. Dynamic imaging of collagen and its modulation in tumors in vivo using second-harmonic generation. *Nature Medicine* **9**:796.
12. Copland, J. A., M. Eghtedari, V. L. Popov, N. Kotov, N. Mamedova, M. Motamedi, and A. A. Oraevsky. 2004. Bioconjugated gold nanoparticles as a molecular based contrast agent: Implications for imaging of deep tumors using optoacoustic tomography. *Molecular Imaging and Biology: MIB: The Official Publication of the Academy of Molecular Imaging* **6**:341.

13. Denk, W., J. H. Strickler, and W. W. Webb. 1990. Two-photon laser scanning fluorescence microscopy. *Science* **248**:73.
14. Dimitrow, E., M. Ziemer, M. J. Koehler, J. Norgauer, K. Konig, P. Elsner, and M. Kaatz. 2009. Sensitivity and specificity of multiphoton laser tomography for in vivo and ex vivo diagnosis of malignant melanoma. *Journal of Investigative Dermatology* **129**:1752.
15. Drachev, V. P., E. N. Khaliullin, W. Kim, F. Alzoubi, S. G. Rautian, V. P. Safonov, R. L. Armstrong, and V. M. Shalaev. 2004. Quantum size effect in two-photon excited luminescence from silver nanoparticles. *Physical Review B* **69**:035318.
16. Drexler, W. 2004. Ultrahigh-resolution optical coherence tomography. *Journal of Biomedical Optics* **9**:47–74.
17. Durr, N. J., T. Larson, D. K. Smith, B. A. Korgel, K. Sokolov, and A. Ben-Yakar. 2007. Two-photon luminescence imaging of cancer cells using molecularly targeted gold nanorods. *Nano Letters* **7**:941.
18. Durr, N. J., C. T. Weisspfennig, B. A. Holfeld, and A. Ben-Yakar. 2011. Maximum imaging depth of two-photon autofluorescence microscopy in epithelial tissues. *Journal of Biomedical Optics* **16**:026008.
19. El-Sayed, I. H., X. Huang, and M. A. El-Sayed. 2006. Selective laser photo-thermal therapy of epithelial carcinoma using anti-EGFR antibody conjugated gold nanoparticles. *Cancer Letters* **239**:129.
20. El-Sayed, I. H., X. Huang, and M. A. El-Sayed. 2005. Surface plasmon resonance scattering and absorption of anti-EGFR antibody conjugated gold nanoparticles in cancer diagnostics: Applications in oral cancer. *Nano Letters* **5**:829.
21. El-Sayed, M. A. 2001. Some interesting properties of metals confined in time and nanometer space of different shapes. *Accounts of Chemical Research* **34**:257.
22. Elghanian, R., J. J. Storhoff, R. C. Mucic, R. L. Letsinger, and C. A. Mirkin. 1997. Selective colorimetric detection of polynucleotides based on the distance-dependent optical properties of gold nanoparticles. *Science* **277**:1078.
23. Frangioni, J. V. 2006. Translating in vivo diagnostics into clinical reality. *Nature Biotechnology* **24**:909.
24. Gambichler, T., G. Moussa, M. Sand, D. Sand, P. Altmeyer, and K. Hoffmann. 2005. Applications of optical coherence tomography in dermatology. *Journal of Dermatological Science* **40**:85–94.
25. Garcia, M., A. Jemal, E. M. Ward, M. M. Center, Y. Hao, R. I. Siegel, and M. J. Thun. 2007. Global cancer facts and figures 2007.
26. Ghosn, B., A. L. van de Ven, J. Tam, A. Gillenwater, K. V. Sokolov, R. Richards-Kortum, and K. Roy. 2010. Efficient mucosal delivery of optical contrast agents using imidazole-modified chitosan. *Journal of Biomedical Optics* **15**:015003.
27. Hirsch, L. R., R. J. Stafford, J. A. Bankson, S. R. Sershen, B. Rivera, R. E. Price, J. D. Hazle, N. J. Halas, and J. L. West. 2003. Nanoshell-mediated near-infrared thermal therapy of tumors under magnetic resonance guidance. *Proceedings of the National Academy of Sciences of the United States of America* **100**:13549.
28. Horisberger, M. and J. Rosset. 1977. Colloidal gold, a useful marker for transmission and scanning electron-microscopy. *Journal of Histochemistry & Cytochemistry* **25**:295–305.
29. Hoy, C., N. Durr, P. Y. Chen, D. K. Smith, T. Larson, W. Piyawattanametha, H. J. Ra, B. Korgel, K. Sokolov, O. Solgaard, and A. Ben-Yakar. 2008. Two-photon luminescence imaging using a MEMS-based miniaturized probe. *Conference on Lasers and Electro-Optics and Quantum Electronics and Laser Science Conference* **1–9**:951–952.
30. Hoy, C. L., N. J. Durr, P. Chen, W. Piyawattanametha, H. Ra, O. Solgaard, and A. Ben-Yakar. 2008. Miniaturized probe for femtosecond laser microsurgery and two-photon imaging. *Optics Express* **16**:9996.
31. Huang, X., I. H. El-Sayed, W. Qian, and M. A. El-Sayed. 2006. Cancer cell imaging and photothermal therapy in the near-infrared region by using gold nanorods. *Journal of the American Chemical Society* **128**:2115.
32. Huang, X., S. Neretina, and M. A. El-Sayed. 2009. Gold nanorods: From synthesis and properties to biological and biomedical applications. *Advanced Materials* **21**:4880.
33. Imura, K., T. Nagahara, and H. Okamoto. 2004. Plasmon mode imaging of single gold nanorods. *Journal of the American Chemical Society* **126**:12730–12731.
34. Jain, P. K., K. S. Lee, I. H. El-Sayed, and M. A. El-Sayed. 2006. Calculated absorption and scattering properties of gold nanoparticles of different size, shape, and composition: Applications in biological imaging and biomedicine. *Journal of Physical Chemistry B* **110**:7238.

35. Kneipp, K., A. S. Haka, H. Kneipp, K. Badizadegan, N. Yoshizawa, C. Boone, K. E. Shafer-Peltier, J. T. Motz, R. R. Dasari, and M. S. Feld. 2002. Surface-enhanced Raman spectroscopy in single living cells using gold nanoparticles. *Applied Spectroscopy* **56**:150.
36. Konig, K. 2000. Multiphoton microscopy in life sciences. *Journal of Microscopy-Oxford* **200**:83–104.
37. Kort, E. J., N. Paneth, and G. F. Vande Woude. 2009. The decline in U.S. cancer mortality in people born since 1925. *Cancer Research* **69**:6500.
38. Kumar, V., N. Fausto, and A. Abbas. 2004. *Robbins & Cotran Pathologic Basis of Disease*, 7th edn. Saunders, Philadelphia, PA. AQ8
39. König, K. and I. Riemann. 2003. High-resolution multiphoton tomography of human skin with subcellular spatial resolution and picosecond time resolution. *Journal of Biomedical Optics* **8**:432–439.
40. König, K., M. Speicher, R. Bückle, J. Reckfort, G. McKenzie, J. Welzel, M. J. Koehler, P. Elsner, and M. Kaatz. 2009. Clinical optical coherence tomography combined with multiphoton tomography of patients with skin diseases. *Journal of Biophotonics* **2**:389.
41. Lakowicz, J. R. 2006. *Principles of Fluorescence Spectroscopy*. Springer, New York.
42. Larson, D. R., W. R. Zipfel, R. M. Williams, S. W. Clark, M. P. Bruchez, F. W. Wise, and W. W. Webb. 2003. Water-soluble quantum dots for multiphoton fluorescence imaging in vivo. *Science* **300**:1434.
43. Lewinski, N., V. Colvin, and R. Drezek. 2008. Cytotoxicity of nanoparticles. *Small* **4**:26.
44. Liu, C.-L., M.-L. Ho, Y.-C. Chen, C.-C. Hsieh, Y.-C. Lin, Y.-H. Wang, M.-J. Yang, H.-S. Duan, B.-S. Chen, J.-F. Lee, J.-K. Hsiao, and P.-T. Chou. 2009. Thiol-functionalized gold nanodots: Two-photon absorption property and imaging in vitro. *The Journal of Physical Chemistry C* **113**:21082.
45. Loo, C., A. Lowery, N. Halas, J. West, and R. Drezek. 2005. Immunotargeted nanoshells for integrated cancer imaging and therapy. *Nano Letters* **5**:709.
46. Mallidi, S., T. Larson, J. Aaron, K. Sokolov, and S. Emelianov. 2007. Molecular specific optoacoustic imaging with plasmonic nanoparticles. *Optics Express* **15**:6583.
47. Masters, B. R., P. T. So, and E. Gratton. 1997. Multiphoton excitation fluorescence microscopy and spectroscopy of in vivo human skin. *Biophysical Journal* **72**:2405.
48. Mitamura, K. and T. Imae. 2009. Functionalization of gold nanorods toward their applications. *Plasmonics* **4**:23–30.
49. Mohamed, M. B., V. Volkov, S. Link, and M. A. El-Sayed. 2000. The 'lightning' gold nanorods: Fluorescence enhancement of over a million compared to the gold metal. *Chemical Physics Letters* **317**:517.
50. Mooradian, A. 1969. Photoluminescence of metals. *Physical Review Letters* **22**:185.
51. Nabiev, I. R., H. Morjani, and M. Manfait. 1991. Selective analysis of antitumor drug interaction with living cancer cells as probed by surface-enhanced Raman spectroscopy. *European Biophysics Journal* **19**:311–316.
52. Niidome, T., M. Yamagata, Y. Okamoto, Y. Akiyama, H. Takahashi, T. Kawano, Y. Katayama, and Y. Niidome. 2006. PEG-modified gold nanorods with a stealth character for in vivo applications. *Journal of Controlled Release* **114**:343.
53. Norman, R. S., J. W. Stone, A. Gole, C. J. Murphy, and T. L. Sabo-Attwood. 2008. Targeted photothermal lysis of the pathogenic bacteria, *Pseudomonas aeruginosa*, with gold nanorods. *Nano Letters* **8**:302.
54. O'Neal, D. P., L. R. Hirsch, N. J. Halas, J. D. Payne, and J. L. West. 2004. Photo-thermal tumor ablation in mice using near infrared-absorbing nanoparticles. *Cancer Letters* **209**:171.
55. Oldenburg, A. L., M. N. Hansen, D. A. Zweifel, A. Wei, and S. A. Boppart. 2006. Plasmon-resonant gold nanorods as low backscattering albedo contrast agents for optical coherence tomography. *Optics Express* **14**:6724.
56. Paoli, J., M. Smedh, and M. B. Ericson. 2009. Multiphoton laser scanning microscopy—A novel diagnostic method for superficial skin cancers. *Seminars in Cutaneous Medicine and Surgery* **28**:190–195.
57. Park, J., A. Estrada, K. Sharp, K. Sang, J. A. Schwartz, D. K. Smith, C. Coleman, J. D. Payne, B. A. Korgel, A. K. Dunn, and J. W. Tunnell. 2008. Two-photon-induced photoluminescence imaging of tumors using near-infrared excited gold nanoshells. *Optics Express* **16**:1590.
58. Raab, S. S., D. M. Grzybicki, J. E. Janosky, R. J. Zarbo, F. A. Meier, C. Jensen, and S. J. Geyer. 2005. Clinical impact and frequency of anatomic pathology errors in cancer diagnoses. *Cancer* **104**:2205–2213.
59. Rajadhyaksha, M., M. Grossman, D. Esterowitz, R. H. Webb, and R. R. Anderson. 1995. In vivo confocal scanning laser microscopy of human skin: Melanin provides strong contrast. *Journal of Investigative Dermatology* **104**:946.

60. Rallan, D. and C. C. Harland. 2003. Ultrasound in dermatology—Basic principles and applications. *Clinical and Experimental Dermatology* **28**:632–638.
61. Rayavarapu, R. G., W. Petersen, L. Hartsuiker, P. Chin, H. Janssen, F. W. B. van Leeuwen, C. Otto, S. Manohar, and T. G. van Leeuwen. 2010. In vitro toxicity studies of polymer-coated gold nanorods. *Nanotechnology* **21**:145101.
62. Sau, T. K. and C. J. Murphy. 2004. Seeded high yield synthesis of short Au nanorods in aqueous solution. *Langmuir* **20**:6414–6420.
63. Schlessinger, J. 2000. Cell signaling by receptor tyrosine kinases. *Cell* **103**:211–225.
64. Schultz, S., D. R. Smith, J. J. Mock, and D. A. Schultz. 2000. Single-target molecule detection with nonbleaching multicolor optical immunolabels. *Proceedings of the National Academy of Sciences of the United States of America* **97**:996.
65. Skala, M. C., M. J. Crow, A. Wax, and J. A. Izatt. 2008. Photothermal optical coherence tomography of epidermal growth factor receptor in live cells using immunotargeted gold nanospheres. *Nano Letters* **8**:3461.
66. Sokolov, K., M. Follen, J. Aaron, I. Pavlova, A. Malpica, R. Lotan, and R. Richards-Kortum. 2003. Real-time vital optical imaging of precancer using anti-epidermal growth factor receptor antibodies conjugated to gold nanoparticles. *Cancer Research* **63**:1999.
67. Sonnichsen, C. and A. P. Alivisatos. 2005. Gold nanorods as novel nonbleaching plasmon-based orientation sensors for polarized single-particle microscopy. *Nano Letters* **5**:301.
68. Sun, C. K., F. Vallee, L. H. Acioli, E. P. Ippen, and J. G. Fujimoto. 1994. Femtosecond-tunable measurement of electron thermalization in gold. *Physical Review B* **50**:15337.
69. Takahashi, H., Y. Niidome, T. Niidome, K. Kaneko, H. Kawasaki, and S. Yamada. 2006. Modification of gold nanorods using phospatidylcholine to reduce cytotoxicity. *Langmuir* **22**:2.
70. Tong, L., Q. Wei, A. Wei, and J.-X. Cheng. 2009. Gold nanorods as contrast agents for biological imaging: Optical properties, surface conjugation and photothermal effects. *Photochemistry and Photobiology* **85**:21.
71. Turkevich, J., P. C. Stevenson, and J. Hillier. 1953. The formation of colloidal gold. *The Journal of Physical Chemistry* **57**:670.
72. Wang, H., T. B. Huff, D. A. Zweifel, W. He, P. S. Low, A. Wei, and J. X. Cheng. 2005. In vitro and in vivo two-photon luminescence imaging of single gold nanorods. *Proceedings of the National Academy of Sciences* **102**:15752.
73. Wilcoxon, J. P., J. E. Martin, F. Parsapour, B. Wiedenman, and D. F. Kelley. 1998. Photoluminescence from nanosize gold clusters. *Journal of Chemical Physics* **108**:9137.
74. Xu, C. and W. W. Webb. 1996. Measurement of two-photon excitation cross sections of molecular fluorophores with data from 690 to 1050 nm. *Journal of the Optical Society of America B—Optical Physics* **13**:481.
75. Xu, M. H. and L. H. V. Wang. 2006. Photoacoustic imaging in biomedicine. *Review of Scientific Instruments* **77**:1–22.
76. Yasuda, R., H. Noji, M. Yoshida, K. Kinosita, and H. Itoh. 2001. Resolution of distinct rotational substeps by submillisecond kinetic analysis of F1-ATPase. *Nature* **410**:898.
77. Yelin, D., D. Oron, S. Thiberge, E. Moses, and Y. Silberberg. 2003. Multiphoton plasmon-resonance microscopy. *Optics Express* **11**:1385.
78. Zhang, E. Z., J. G. Laufer, R. B. Pedley, and P. C. Beard. 2009. In vivo high-resolution 3D photoacoustic imaging of superficial vascular anatomy. *Physics in Medicine and Biology* **54**:1035.
79. Zhang, H. F., K. Maslov, G. Stoica, and L. V. Wang. 2006. Functional photoacoustic microscopy for high-resolution and noninvasive in vivo imaging. *Nature Biotechnology* **24**:848.
80. Zipfel, W. R., R. M. Williams, R. Christie, A. Y. Nikitin, B. T. Hyman, and W. W. Webb. 2003. Live tissue intrinsic emission microscopy using multiphoton-excited native fluorescence and second harmonic generation. *Proceedings of the National Academy of Sciences* **100**:7075.
81. Zipfel, W. R., R. M. Williams, and W. W. Webb. 2003. Nonlinear magic: Multiphoton microscopy in the biosciences. *Nature Biotechnology* **21**:1368.

AUTHOR QUERIES

[AQ1] Please check the shortened running head "Multiphoton Luminescence from Gold Nanoparticles".
[AQ2] Please check the source line of Figure 17.2 for correctness.
[AQ3] Would you consider changing "hexadecyltrimethylammonium" to "hexadecyl cetyltrimethylammonium"? Please check.
[AQ4] Can all instances of the unit "kD" be changed to "kDa"?
[AQ5] Please check if edit in the sentence starting "While some groups …" is ok.
[AQ6] Please check the edit of the author names in Ref. [10] for correctness.
[AQ7] Please provide complete details for Ref. [25].
[AQ8] Please check the inserted publisher location for Ref. [38].